JACS
JOURNAL OF THE AMERICAN CHEMICAL SOCIETY
Article
pubs.acs.org/JACS

Synthesis, Isotopic Enrichment, and Solid-State NMR Characterization of Zeolites Derived from the Assembly, Disassembly, Organization, Reassembly Process

Giulia P. M. Bignami, Daniel M. Dawson, Valerie R. Seymour, Paul S. Wheatley, Russell E. Morris,* and Sharon E. Ashbrook*

School of Chemistry, EaStCHEM and Centre of Magnetic Resonance, University of St. Andrews, North Haugh, St. Andrews, Fife KY16 9ST, United Kingdom

Supporting Information

ABSTRACT: The great utility and importance of zeolites in fields as diverse as industrial catalysis and medicine has driven considerable interest in the ability to target new framework types with novel properties and applications. The recently introduced and unconventional assembly, disassembly, organization, reassembly (ADOR) method represents one exciting new approach to obtain solids with targeted structures by selectively disassembling preprepared hydrolytically unstable frameworks and then reassembling the resulting products to form materials with new topologies. However, the hydrolytic mechanisms underlying such a powerful synthetic method are not understood in detail, requiring further investigation of the kinetic behavior and the outcome of reactions under differing conditions. In this work, we report the optimized ADOR synthesis, and subsequent solid-state characterization, of ^{17}O- and doubly ^{17}O- and ^{29}Si-enriched UTL-derived zeolites, by synthesis of ^{29}Si-enriched starting Ge-UTL frameworks and incorporation of ^{17}O from ^{17}O-enriched water during hydrolysis. ^{17}O and ^{29}Si NMR experiments are able to demonstrate that the hydrolysis and rearrangement process occurs over a much longer time scale than seen by diffraction. The observation of unexpectedly high levels of ^{17}O in the bulk zeolitic layers, rather than being confined only to the interlayer spacing, reveals a much more extensive hydrolytic rearrangement than previously thought. This work sheds new light on the role played by water in the ADOR process and provides insight into the detailed mechanism of the structural changes involved.

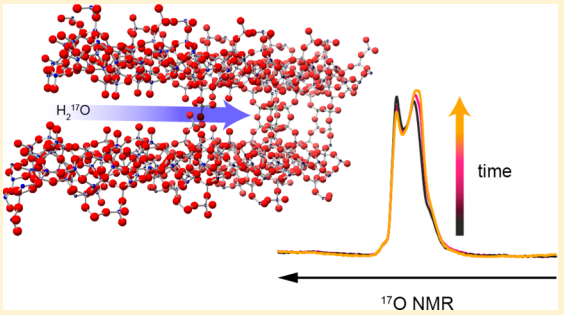

INTRODUCTION

Zeolites are inorganic porous compounds made up of fully cross-linked frameworks of corner-sharing SiO_4 and AlO_4 tetrahedra.[1] Owing to their crystalline structure and porosity, these materials have high surface areas, and so great potential for catalytic activity. They also possess a narrow range of pore sizes of molecular dimensions, leading to their well-known shape selectivity.[2−10] Such a unique combination of structural features accounts for their vast success and variety of applications over the years, and this has kept the targeting of new framework types at the forefront of research.[11−20] The recently introduced assembly, disassembly, organization, reassembly (ADOR) method,[21−25] shown schematically in Figure 1, has proven to be a feasible approach to achieve such a goal, transforming the way new, stable, and active materials can be synthesized. This unconventional synthetic approach is based on the chemically selective disassembly of hydrolytically unstable parent frameworks and their subsequent controlled reassembly into solids with predetermined structures. The key feature characterizing the parent zeolite required for the process is the presence of a hydrolytically sensitive dopant element incorporated within the framework at specific sites, which allows the chemically selective removal of the units that contain the dopant. Germanosilicates are excellent candidates for this process as Ge, which has greater flexibility in its coordination environment than Si, is known to locate preferentially within certain zeolite subunits and, in particular, occupies tetrahedral-atom positions within the double four rings (d4rs).[26−29] Moreover, germanosilicate zeolites have been shown to be much more sensitive to hydrolysis than silica or aluminosilicate materials.[29−31] Using germanosilicates that adopt the UTL[32,33] framework structure as the parent zeolite, ADOR has enabled the preparation of two new zeolite materials, IPC-2 and IPC-4,[21,24] whose topologies have been given the three-letter codes OKO and PCR, respectively, by the International Zeolite Association. It has also allowed the preparation of other new zeolite structures IPC-6, IPC-7, IPC-9, and IPC-10,[23,24,34] and some of these are likely to be difficult, or even impossible, to prepare using standard hydrothermal methods.[35,36]

Controlling the acidity of the solution used to disassemble the parent zeolite in the ADOR process enables different final

Received: January 18, 2017
Published: March 20, 2017

DOI: 10.1021/jacs.7b00386
J. Am. Chem. Soc. 2017, 139, 5140−5148

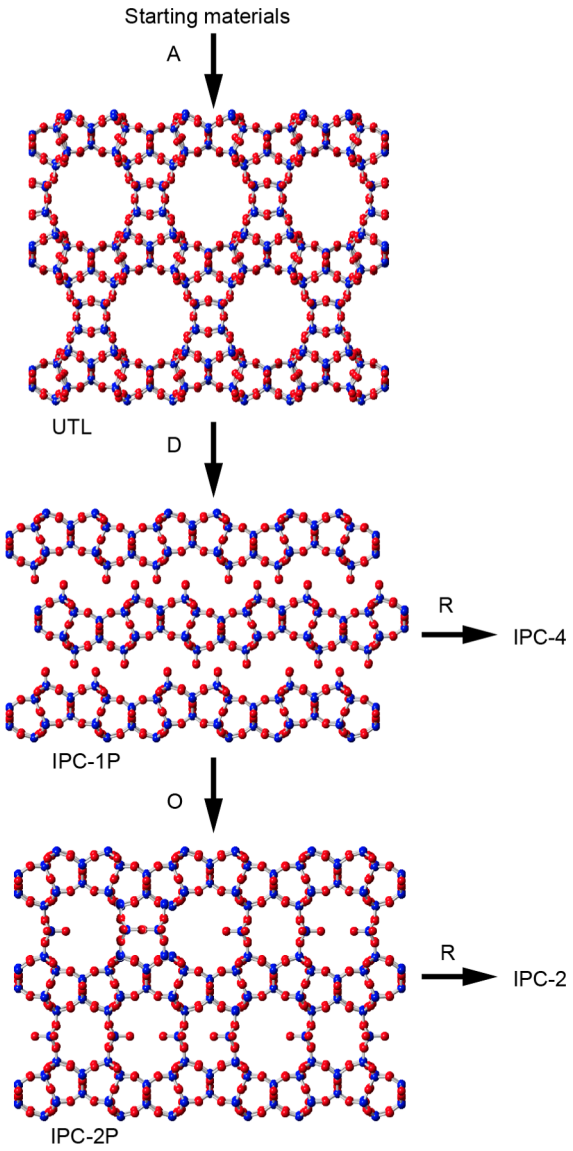

Figure 1. General schematic representation of the ADOR process when using large volumes of hydrolysis solution. A is the assembly step for the preparation of the parent Ge-UTL zeolite. D is the full hydrolysis of the parent material to leave the layered IPC-1P intermediate. Over time, there is an organization (O) process that rearranges the structure to produce a new intermediate material, IPC-2P. Reassembly (R) by calcining the intermediates leads to the fully connected IPC-2 and IPC-4 zeolite structures. Note that the structures of IPC-1P, IPC-4, and IPC-2 are well established in the literature but that IPC-2P is heavily disordered, and the model shown is idealized. Full details of the structures and conditions used for the processes can be found in the literature.[21,24,37] Color key: blue = Si, red = O, except for UTL where blue = Si or Ge.

materials to be effectively targeted and their porosity tuned over a wide range.[24] Such a control over pore volume/surface area is difficult to achieve following traditional approaches to zeolite synthesis, highlighting the notable advance achieved by the development of the ADOR process. However, a better understanding of the hydrolytic mechanisms controlling the ADOR process is required, and, in particular, a more detailed insight of the interaction of the zeolitic framework with water would be beneficial. Thanks to its sensitivity to the local, atomic-scale environment, and its element-specific nature, solid-state NMR spectroscopy can complement other solid-state characterization techniques, such as powder X-ray diffraction (PXRD) and N_2 adsorption, used for the investigation of zeolitic frameworks.[1,38−42] For most silica-based zeolites, ^{17}O and ^{29}Si are the two NMR-active nuclei of most interest. Despite its low natural abundance of 4.7%, ^{29}Si (I = 1/2) is routinely employed for the NMR characterization of zeolites. However, ^{17}O (I = 5/2) is less commonly studied, owing to the anisotropic quadrupolar broadening of the spectral line shapes, very low natural abundance (0.037%), and moderate gyromagnetic ratio.[43,44] To enable a complete and high-resolution spectroscopic investigation of the zeolitic structures of interest in each step of the ADOR process, isotopic enrichment is required. Here, we show how hydrolysis of a ^{29}Si-enriched Ge-UTL zeolite using $H_2{}^{17}O$ can shed new light on the role played by water in the ADOR process and provide insight into the structural changes involved in the mechanism. The work shows that the detailed mechanistic pathway, and so the final products, of the ADOR process depends heavily on the conditions used, including the volume of the solution used to hydrolyze the initial parent zeolite.

EXPERIMENTAL METHODS

Experiments on unenriched zeolites were carried out on materials from a single starting batch of Ge-UTL (Si/Ge ratio of 4.4), which was synthesized and calcined following the procedure in ref 24, but using a shorter reaction time (under static heating conditions) of 7 days. A similar procedure was followed to synthesize ^{29}Si-enriched Ge-UTL, starting from 18% ^{29}Si-enriched TEOS, with a longer overall reaction time of 14 days. The unenriched calcined Ge-UTL starting material was hydrolyzed with water (natural abundance) for different lengths of time. Low-volume reactions were carried out using a 10 mL round-bottomed flask topped with a condenser in refluxing conditions at 95 °C in 6 M HCl (freshly produced from 1.2 mL of natural-abundance water and 1.2 mL of 12 M HCl) for reaction times ranging from 4 to 48 h. For ^{17}O-enriched and doubly ^{17}O- and ^{29}Si-enriched zeolites, hydrolysis was carried out using 6 M HCl (produced from 1.2 mL of water 41% enriched in ^{17}O and 1.2 mL of 12 M HCl) for 16 h. Materials were washed with only a small volume (2.4 mL) of natural-abundance water to minimize any loss of ^{17}O (see the Supporting Information for more detail). Calcination of the hydrolyzed products was carried out to remove any remaining water from hydrolysis and allow the condensation of the hydrolyzed layers in the framework. Typically, the zeolite was heated to 575 °C at a rate of 1 °C/min, held for 6 h, and cooled to room temperature at a rate of 2 °C/min under air.

^{29}Si solid-state NMR spectra were acquired using a Bruker Avance III spectrometer, equipped with a 9.4 T wide-bore superconducting magnet, at a Larmor frequency of 79.459 MHz. Samples were packed into 4 mm ZrO_2 rotors that were rotated at a rate of 10 kHz, using a 4 mm HX probe. Magic angle spinning (MAS) spectra were acquired using a radiofrequency (rf) field strength of ∼83 kHz, with a repeat interval of 120 s. The Q^4/Q^3 ratio was determined using DMFit,[45] with errors estimated from multiple fits. For cross-polarization (CP)[44,46] experiments, transverse magnetization was transferred (from ^1H) using a contact pulse of 5 ms (ramped for ^1H), with two-pulse phase modulation (TPPM) ^1H decoupling (using a rf field strength of ∼70 kHz) during acquisition. The commercial probes used for these experiments exhibited a small ^{29}Si background signal (estimated to be ∼8% of the total signal intensity). No correction has been made to the Q^4/Q^3 ratios plotted in Figure 3 to account for this.

^{17}O solid-state NMR spectra were acquired on Bruker Avance III spectrometers, equipped with 14.1 or 20.0 T wide-bore superconducting magnets, at Larmor frequencies of 81.331 and 115.248 MHz, respectively. Samples were packed into 3.2 mm ZrO_2 rotors and rotated at a rate of 20 kHz. MAS NMR spectra were acquired using a

DOI: 10.1021/jacs.7b00386
J. Am. Chem. Soc. 2017, 139, 5140−5148

rf field strength of ~70 kHz, with a repeat interval of 1 s, using continuous wave (cw) ^{1}H decoupling (~100 kHz) where necessary. For CP experiments, transverse magnetization was transferred (from ^{1}H) using a contact pulse of 1 ms (ramped for ^{1}H), and cw ^{1}H decoupling (~100 kHz) was applied during acquisition. Variable-temperature CP experiments were carried out at the UK DNP MAS NMR Facility at the University of Nottingham. The neat ^{17}O-enriched solid was packed in a sapphire rotor, a contact pulse of 1 ms was used, and swept-frequency TPPM decoupling (~100 kHz) was applied during acquisition. Repeat intervals of 1 and 4.3 s were used for experiments recorded at 298 and 108 K, respectively. ^{17}O MQMAS experiments were carried out using a triple-quantum z-filtered pulse sequence[47,48] and are shown after a shearing transformation.[49] Where desired, cw ^{1}H decoupling was applied. The indirect dimension is scaled and referenced according to the convention described in ref 50. Two-dimensional ^{17}O−^{29}Si heteronuclear correlation spectra were acquired at 20.0 T using a D-HMQC pulse sequence (with 2−8 loops of $SR4^2_1$ recoupling),[51,52] central-transition selective pulses for ^{17}O and cw ^{1}H decoupling (~100 kHz).

Chemical shifts are shown relative to TMS for ^{29}Si and ^{2}H (using Q8M8 ($\delta(OSi(OMe)_3)$ = 11.5 ppm) and $C_2D_2O_4{\cdot}2D_2O$ ($\delta(CO_2D)$ = 16.5 ppm) as secondary references) and H_2O for ^{17}O. See figure captions for further details.

PXRD data were acquired with a PANalytical Empyrean instrument operated in reflection, Bragg−Brentano, θ-2θ mode, and equipped with a Cu X-ray tube, a primary beam monochromator ($CuK_{\alpha 1}$), and X'celerator RTMS detector. Typically, a 5−50° 2θ range was investigated over 1 h. For all isotopically enriched samples, powders were sealed in capillaries, and data were collected on a STOE STADIP instrument operated in Debye−Scherrer mode equipped with a Cu X-ray tube, a primary beam monochromator ($CuK_{\alpha 1}$), and a scintillation position-sensitive linear detector. Typically, 5−50° or 5−40° 2θ ranges were investigated over 1.5 h or overnight, respectively. N_2 volumetric adsorption data were acquired at −196 °C with a Tristar II 3020. Samples were degassed at 300 °C for 3 h prior to the adsorption experiment.

RESULTS AND DISCUSSION

Samples of unenriched Ge-UTL were hydrolyzed, and the resulting products calcined and then characterized using ^{29}Si MAS NMR, PXRD, and N_2 adsorption. Owing to the cost of $H_2{}^{17}O$ and, therefore, the need to reduce the amount of water required, the standard hydrolysis procedure (as reported in ref 24) needed to be scaled to use a low volume of water (i.e., 2.4 mL) for hydrolysis to enable ^{17}O-enriched materials to be produced economically. Hydrolysis reaction times of 4, 8, 12, 16, 24, and 48 h were investigated, initially using unenriched water, as described in the Experimental Methods section. A striking difference between these studies and the large volume studies previously reported is that the formation of the fully hydrolyzed layered intermediate known as IPC-1P (see Figure 1) is not observed.[21,24,37] Under previously reported conditions, IPC-1P can rearrange, with intercalation of extra silicon, into a material called IPC-2P where the layers are connected through O−Si−O links. In the low-volume experiments reported here, there is no evidence of IPC-1P, and at all stages, the intermediates have PXRD patterns with reflection positions consistent with IPC-2P (see the Supporting Information). Calcination of IPC-2P at 575 °C produces materials with similar PXRD patterns to IPC-2, and N_2 adsorption measurements on the calcined samples are consistent with this result (see the Supporting Information), which also demonstrates that the small amounts of washing water used had not affected the porosity of the framework. The observation that IPC-1P is never formed points to a different mechanism in low volumes of hydrolysis solutions compared to that observed in higher volumes. The NMR experiments described in detail below are consistent with these observations.

Figure 2a shows ^{29}Si MAS NMR spectra of the starting Ge-UTL zeolite containing only Q^4 ($\mathbf{Si}(OSi)_n(OGe)_{4-n}$) species.

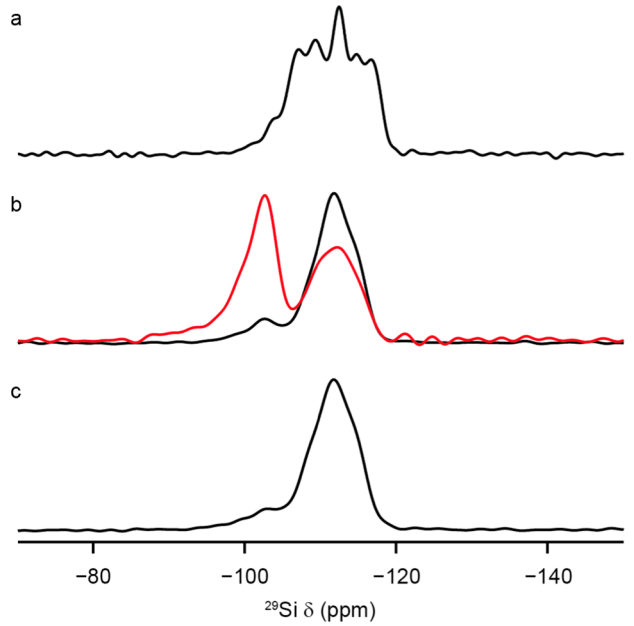

Figure 2. ^{29}Si (9.4 T, 10 kHz MAS) NMR spectra of (a) calcined Ge-UTL starting zeolite, (b) after 16 h hydrolysis, and (c) after subsequent calcination. In (b), the ^{29}Si (9.4 T, 10 kHz MAS) CP NMR spectrum is also shown (in red).

CP MAS spectra of this sample contain no signal, confirming no Q^3 species are present. Figure 2b shows the spectrum after 16 h hydrolysis, where both Q^4 ($Si(OSi)_4$) and Q^3 ($\mathbf{Si}(OSi)_3(OH)$) species are present, suggesting the formation of Si−OH groups. The spectral assignment was confirmed using a CP MAS experiment, shown by the red line in Figure 2b, where selective enhancement of the peak at δ = −102 ppm is observed. After calcination, the relative intensities of the resonances corresponding to Q^4 and Q^3 species vary slightly, as shown in Figure 2c, suggesting some Si−OH remain as defects (and confirmed using CP experiments). Unlike the diffraction measurements, the ^{29}Si MAS NMR spectra of the zeolites do show a change with hydrolysis time, revealing an ongoing hydrolysis and rearrangement process, which is difficult to see in the average picture provided by PXRD (see the Supporting Information). Figure 3a shows a plot of the ratio of the intensities of the Q^4 and Q^3 species in the hydrolyzed samples as the reaction proceeds. An initial hydrolytic stage is observed with an increase in the amount of Q^3 (i.e., Si−OH) sites, and a subsequent decrease in the Q^4/Q^3 ratio, until 12 h of reaction. However, Q^4/Q^3 never reaches the ideal number expected for the IPC-1P intermediate (Q^4/Q^3 = 2.5, red dashed line in Figure 3a) instead reaching a minimum Q^4/Q^3 of just over 4. This is consistent with the XRD results described above. After this point, a rearrangement process (similar to that observed in previous work)[53] begins, resulting in a Q^4/Q^3 ratio that increases until it reaches the expected value for the idealized structure of IPC-2P (Q^4/Q^3 = 7, blue dashed line in Figure 3a). This suggests that, under the low volume conditions described here, the initial hydrolysis process never reaches its conclusion before the rearrangement phase of the reaction begins. The

DOI: 10.1021/jacs.7b00386
J. Am. Chem. Soc. 2017, 139, 5140−5148

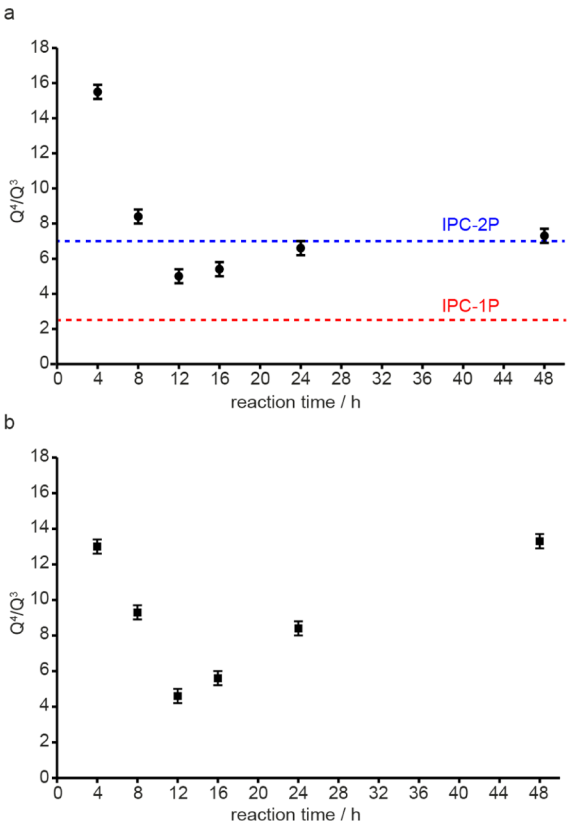

Figure 3. Plots of the Q^4/Q^3 intensity ratio in ^{29}Si (9.4 T, 10 kHz MAS) NMR spectra of Ge-UTL zeolite as a function of hydrolysis time under low-volume conditions for samples (a) as prepared and (b) after calcination. In (a), the red and blue dashed lines show the Q^4/Q^3 ratios for idealized IPC-1P (2.5) and IPC-2P (7), respectively. Error bars have been estimated from multiple fits.

relatively constant PXRD patterns for all reaction times after 12 h of reaction indicate that the interlayer spacing does not change significantly after this time, but the variation in Q^4/Q^3 ratio means that there are still significant changes occurring in the local structure throughout the process. Experiments carried out with larger volumes of washing water proved the repeatability and robustness of these results (see the Supporting Information).

Figure 3b shows a plot of the ratio of the intensities of the Q^4 and Q^3 species after calcination of the samples shown in Figure 3a. All samples show the expected PXRD patterns for IPC-2. At the shorter time scales the Q^4/Q^3 values are approximately the same as the hydrolyzed samples, but the rearrangement process (from 12 h onward) leads to calcined IPC-2 samples that have successively fewer defects (higher Q^4/Q^3 values). We denote the disordered/defective nature of the zeolites formed at shorter times by an asterisk − IPC-2P* for the intermediate and IPC-2* for the final zeolite after reassembly.

In order to improve sensitivity, enable multidimensional spectroscopic characterization, and provide insight into the ADOR mechanism, two isotopically enriched zeolites were produced. The first involved the hydrolysis (i.e., disassembly) of Ge-UTL using small volumes of (41% enriched) $H_2{}^{17}O$, as described in the Experimental Methods section. In addition, a zeolite sample doubly enriched in ^{17}O and ^{29}Si was prepared by a 16 h hydrolysis (using $H_2{}^{17}O$) of a starting Ge-UTL zeolite synthesized with (18%) ^{29}Si-enriched TEOS.

These materials were confirmed as being IPC-2P by PXRD (as shown in the Supporting Information). Successful ^{17}O enrichment was also demonstrated using ^{17}O MAS NMR. The ^{17}O MAS NMR spectra of the hydrolyzed ^{17}O-enriched sample, shown in Figure 4, reveal that structural changes occur over a

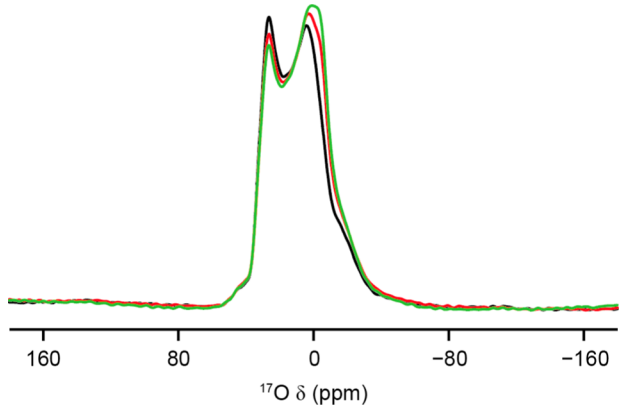

Figure 4. ^{17}O (14.1 T, 20 kHz MAS) NMR spectra of Ge-UTL hydrolyzed with ^{17}O-enriched H_2O for 16 h, acquired 2 (black line), 16 (red line), and 30 (green line) days after synthesis.

long period after synthesis, with variation in the line shape still apparent after 30 days (during which period the sample remained packed within the NMR rotor at room temperature). After this point, no further change was observed. This indicates that the hydrolysis/rearrangement process continues even at room temperature. Two chemically different types of oxygens are present in the material: "bulk" Si−O−Si species and Si−OH species found in the interlayer regions after hydrolysis. The Si−O−Si species can be further categorized by their local environment as described below. It might be expected that the enrichment level of the interlayer Si−OH groups would be much higher as they are formed by direct hydrolysis in the disassembly step of the ADOR process. The use of enriched $H_2{}^{17}O$ provides the opportunity to gain further insight into the mechanism of hydrolysis if the position and proportion of enrichment can be determined and/or quantified.

Owing to the second-order quadrupolar broadening in the ^{17}O ($I = 5/2$) MAS NMR spectrum, it is difficult to resolve the different species that contribute to the line shape.[43,44] Resolution can be improved using MQMAS experiments,[47,48] where resonances are separated in the δ_1 dimension (after appropriate processing) on the basis of their isotropic chemical shifts and quadrupolar shifts (and, therefore, their quadrupolar coupling). As the second-order quadrupolar broadening is inversely proportional to field strength, the resolution observed will vary as B_0 changes.[43,44] Figure 5 shows ^{17}O MQMAS NMR spectra of the ^{17}O-enriched zeolite, acquired at 20.0 T, without and with ^1H decoupling. (MAS and MQMAS spectra acquired at different B_0 field strengths are shown in the Supporting Information.) A resonance is observed in both MQMAS spectra at $\delta_1 \approx 25$ ppm, with $\langle P_Q \rangle \approx 5.3$ MHz, and $\langle \delta_{iso} \rangle \approx 39$ ppm, although a distribution in parameters is apparent. (Note that P_Q[43,44] is a combined quadrupolar parameter (see Supporting Information) and is given by $C_Q(1 + \eta_Q{}^2/3)^{1/2}$ and δ_{iso} is the isotropic chemical shift.) These values are also supported by the fitting of cross sections extracted from the MQMAS spectra, as discussed in the Supporting Information. The decoupled MQMAS spectrum (Figure 5b) shows an additional, lower

DOI: 10.1021/jacs.7b00386
J. Am. Chem. Soc. 2017, 139, 5140−5148

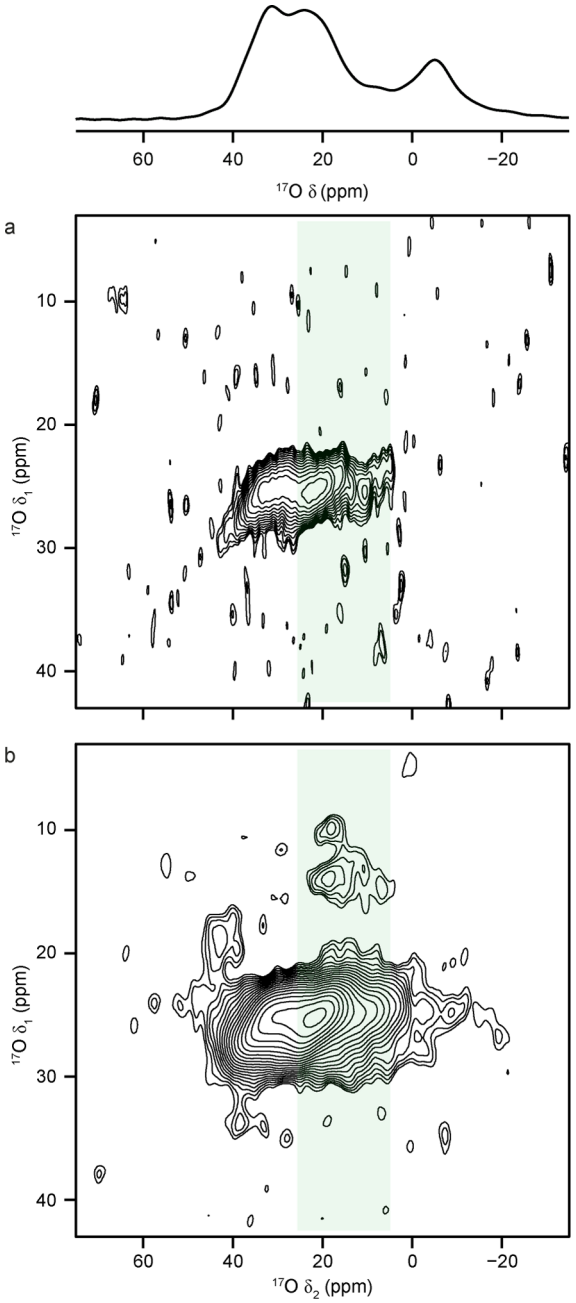

Figure 5. ^{17}O (20.0 T, 20 kHz MAS) triple-quantum NMR spectra of Ge-UTL hydrolyzed with ^{17}O-enriched H_2O for 16 h, acquired using a z-filtered pulse sequence (a) without and (b) with cw ^{1}H decoupling. The total acquisition times were (a) 7 and (b) 22 h. Also shown (above) is the ^{17}O MAS NMR spectrum. The position of the signal seen in CP experiments is highlighted in green.

intensity, resonance at $\delta_1 \approx 13$ ppm, assumed to result from Si−OH species. It is difficult to extract accurate NMR parameters for this resonance, owing to the low sensitivity and lack of any characteristic quadrupolar broadening, but the position of the center of gravity would suggest that $\langle P_Q \rangle \approx 3.4$ MHz and $\langle \delta_{iso} \rangle \approx 23$ ppm. The sharp peak at $\delta = -5.1$ ppm in the MAS spectrum (also shown in Figure 5), which does not appear in the MQMAS spectrum, can be attributed to water. The position of this signal varies very little with the B_0 field, suggesting a negligible quadrupolar interaction, as discussed in the Supporting Information.

To confirm the assignment of the ^{17}O MAS and MQMAS NMR spectra, CP experiments were performed. This approach should edit the spectrum on the basis of spatial proximity to ^{1}H, preferentially enhancing the Si−OH species (as observed for ^{29}Si in Figure 2b). However, CP to quadrupolar nuclei is a much more challenging experiment than its spin $I = 1/2$ counterpart, with multiple match conditions of differing intensity and with sensitivity also depending crucially on the spin-lock efficiency (determined by the adiabaticity parameter, α, which depends on the rf field strength of the spin-lock pulse, the quadrupolar coupling, and the MAS rate).[54−56] Consequently, the CP match condition was initially optimized using a model system (amorphous SiO_2 enriched in ^{17}O), as described in detail in the Supporting Information. From these experiments, a low-power match condition (enabling spin-locking in the sudden regime, where $\alpha \ll 1$) was selected.

As shown in Figure 6, ^{17}O CP MAS NMR spectra (red lines) of the hydrolyzed ^{17}O-enriched sample do show selective

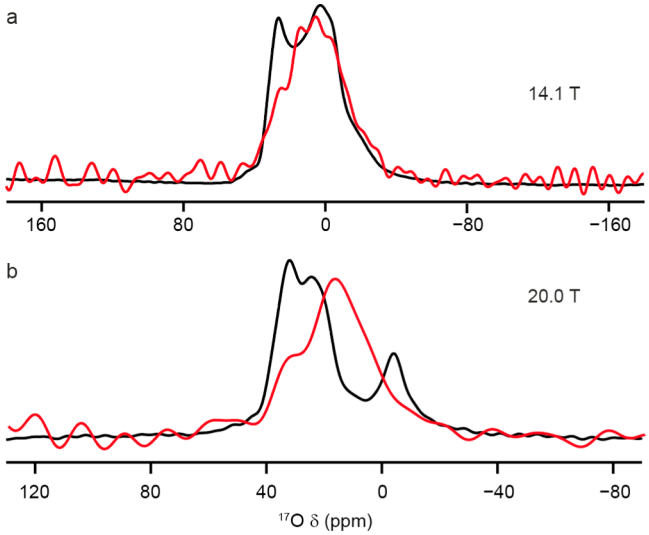

Figure 6. ^{17}O (20 kHz MAS) CP NMR spectra (red) of Ge-UTL hydrolyzed with ^{17}O-enriched H_2O for 16 h, acquired at (a) 14.1 T and (b) 20.0 T. Corresponding MAS spectra are also shown (black) for comparison.

enhancement of the Si−OH signal, with the position of the peak maximum observed at 20.0 T in good agreement with the weak signal resolved in the ^{1}H-decoupled MQMAS spectrum in Figure 5b (as shown by the green box in Figure 5), thus confirming its assignment to Si−OH species. The poor sensitivity of these experiments, even after lengthy acquisition times (3 days at 14.1 T and 13 h at 20.0 T), possibly suggests rapid $T_{1\rho}$ relaxation and/or poor spin-locking behavior. However, as shown in the Supporting Information, the ^{1}H $T_{1\rho}$ relaxation is certainly sufficient for CP at the contact times used, and the Si−OH species exhibit better ^{17}O spin-locking efficiency at the rf fields applied than the Si−O−Si or water species, confirming this is not responsible for the poor CP efficiency observed. Given these observations, it is most likely that the reduced efficiency of CP results from reduction of the dipolar interaction that mediates the magnetization transfer, most probably as a result of motion. Evidence for H dynamics in the hydrolyzed zeolite structure is provided via ^{2}H NMR, as shown in Figure 7 and discussed further in the Supporting Information.

DOI: 10.1021/jacs.7b00386
J. Am. Chem. Soc. 2017, 139, 5140−5148

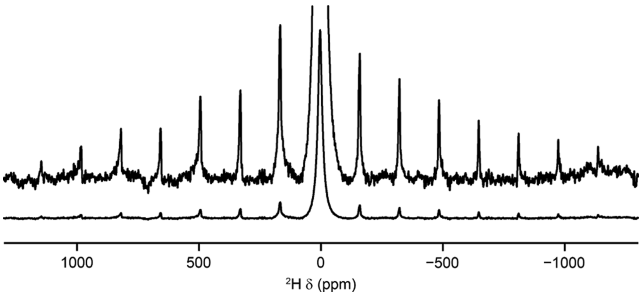

Figure 7. ^{2}H (9.4 T, 10 kHz MAS) NMR spectra of a deuterated ^{17}O-enriched hydrolyzed (16 h) Ge-UTL zeolite, with an expansion to show the broad spinning sideband manifold.

The ^{2}H MAS spectrum is dominated by a narrow, isotropic line shape, suggesting rapidly reorienting D_2O is present between the layers. A broad spinning sideband manifold, corresponding to Si−OD in the interlayer space, is also observed, although this cannot be simulated with just a single quadrupolar line shape, suggesting it is also affected by dynamics, and possibly suggesting H/D exchange with water. From the ^{2}H MAS NMR spectra, it can be estimated that the intensity ratio of the Si−OD:D_2O signal is ∼1:4 (suggesting a 1:2 ratio of silanol groups to molecular water). It seems reasonable to assume this water results from D_2O in the interlayer space and not from surface water (given that samples are dried prior to study and CP to the interlayer Si−OH species appears to be affected by dynamics). However, we note that it is difficult to rule out completely the presence of any strongly bound surface water. The levels of water in the hydrolyzed zeolites vary with hydrolysis duration and storage time and conditions. From the samples studied in this work, the Si−OH:H_2O ratio is estimated to be between 1:2 and 1:4. Further support for the modulation of the dipolar interaction being responsible for the poor CP efficiency is provided by the low-temperature (108 K) CP spectrum in Figure 8. A significant

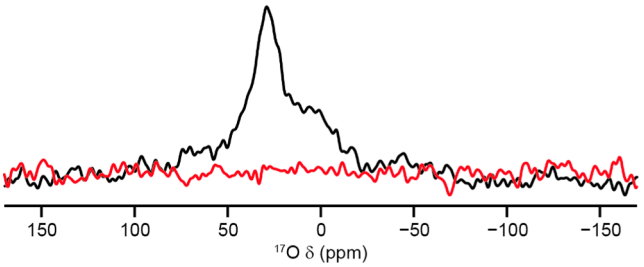

Figure 8. ^{17}O (14.1 T, 12.5 kHz MAS) CP NMR spectra of ^{17}O-enriched hydrolyzed Ge-UTL zeolite, hydrolyzed for 16 h, acquired at 108 K (black line) and 298 K (red line).

increase in CP efficiency is observed at the lower temperature, with a corresponding change in line shape resulting from the restriction or removal of any dynamics.

From the cross sections extracted from MQMAS experiments (for Si−O−Si species) and the line shapes observed in CP and spin-lock experiments, where primarily Si−OH species are observed, it is possible to estimate the relative proportions of different O species present in the hydrolyzed Ge-UTL from fitting a quantitative (i.e., short flip angle) ^{17}O MAS NMR spectrum. As shown in the Supporting Information, the ratio of Si−^{17}O−Si:Si−^{17}O−H:$H_2{}^{17}O$ species is ∼8:1:1. The amount of water present varies between samples hydrolyzed for different durations and those stored for different times under different conditions. One can broadly categorize the oxygen atoms in IPC-2P into four groups (Figure 9): the Si−OH oxygen atoms

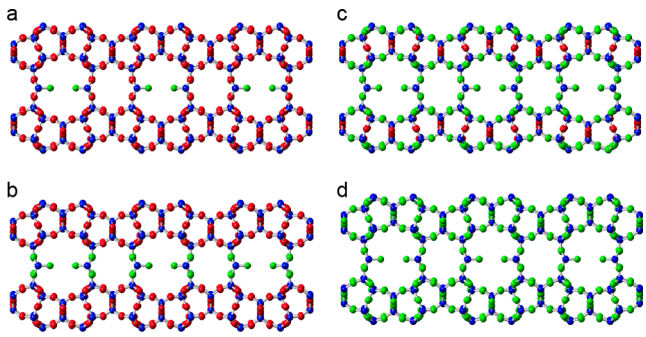

Figure 9. A schematic showing hypothetical models of the most likely ^{17}O incorporation patterns into idealized IPC-2P after hydrolysis with ^{17}O-enriched water. The models are (a) where only the Si−OH groups contain ^{17}O; (b) where ^{17}O is incorporated into the Si−OH and Si−O−Si units in the interlayer units (expected Si−^{17}O−Si:Si−^{17}OH ratio is 2.5:1); (c) where ^{17}O is incorporated into Si−OH units, Si−O−Si in the interlayer unit, and into the first layer of tetrahedra in the layers (expected Si−^{17}O−Si:Si−^{17}OH is 11.5:1); and (d) where ^{17}O is equally likely to be incorporated into all possible oxygen sites in the structure (expected Si−^{17}O−Si:Si−^{17}OH is 16.5:1). Green spheres are oxygen atoms with a high probability of ^{17}O incorporation, and red spheres indicate a low probability of ^{17}O incorporation. Silicon is shown in blue. Note that experiments also indicate water is present in the interlayer region, but this is not shown.

and three different types of Si−O−Si units; those in the interlayer region, those in the layers but which are accessible to the pore spaces, and those in the layers that are not accessible to the pores. Using the models shown in Figure 9, one can calculate the expected ratio of Si−^{17}O−Si:Si−^{17}OH based on the distributions shown. This is a rather crude calculation as it takes no account of any difference in probability of any particular site being occupied by ^{17}O preferentially over another, but one thing is clear, the observed Si−^{17}O−Si:Si−^{17}OH ratio of ∼8:1 cannot be explained by incorporation into only the interlayer oxygen sites (expected ratio = 2.5:1), and, at the very least, the organization/rearrangement step in the ADOR process involves oxygen atoms being introduced into the layers (for example, the model shown in Figure 9c). This observation is unexpected and, even when considering that any back exchange may be more rapid for Si−OH species, suggests a much more substantial rearrangement process during hydrolysis than previously thought.[21−25] The identification of these resonances also provides insight into the changes seen previously in the ^{17}O MAS spectrum in Figure 4, with the Si−O−Si signal reversibly hydrolyzed to form Si−O−H. Although the low intensity of the Si−OH signal in the MQMAS experiments prevents accurate analysis of the relative proportions of each signal at each stage, it is possible to estimate the relative proportions of different O species present in the three ^{17}O MAS spectra of hydrolyzed Ge-UTL shown. As discussed in the Supporting Information, the proportion of Si−OH increases with time, while that of Si−O−Si decreases, confirming low-level hydrolysis continues even at room temperature, most likely as a result of a small amount of acid remaining between the layers, owing to the reduced volume of (unenriched) washing water used.

DOI: 10.1021/jacs.7b00386
J. Am. Chem. Soc. 2017, 139, 5140−5148

This surprising conclusion was investigated further by the preparation of an IPC-2P sample doubly enriched in both ^{17}O (during a 16 h hydrolysis) and ^{29}Si (from the initial Ge-UTL synthesis). Figure 10 shows $^{17}O-^{29}Si$ HMQC correlation spectra of this doubly enriched sample (acquired at 20.0 T, with $SR4^2_1$ recoupling of the Si−O dipolar interaction).[51,52] At short recoupling times, the spectrum contains signal only from Si−O−Si coordinated to Q^4 Si species, while at longer times, the same ^{17}O species correlate with the Q^3 Si (i.e., Si−OH) groups, confirming these lie in the bulk of the zeolite layers and at a greater distance to the interlayer spaces. Although little signal is seen from any Si−O−Si coordinated to Q^3 Si species within the interlayer regions, there are proportionately fewer of these (and fewer still in the more defective IPC-2P* material), and these might also experience more rapid relaxation, owing to their proximity to the dynamic interlayer water.

In both spectra, there is no correlation of the ^{17}O signal at $\delta \approx -6.4$ ppm with any Si species, confirming it as nonstructural water. Interestingly, there are also no signals in the spectrum in the region where the CP experiments indicated the Si−OH species could be seen. This probably also results from rapid relaxation during the transfer step, as suggested above. Even if some back exchange of Si−OH species does occur when a sample is stored under ambient conditions, perturbing the relative intensities of the species, Figure 10, confirms a significant proportion of ^{17}O resides in the bulk zeolite layers, rather than being restricted only to the interlayer regions.

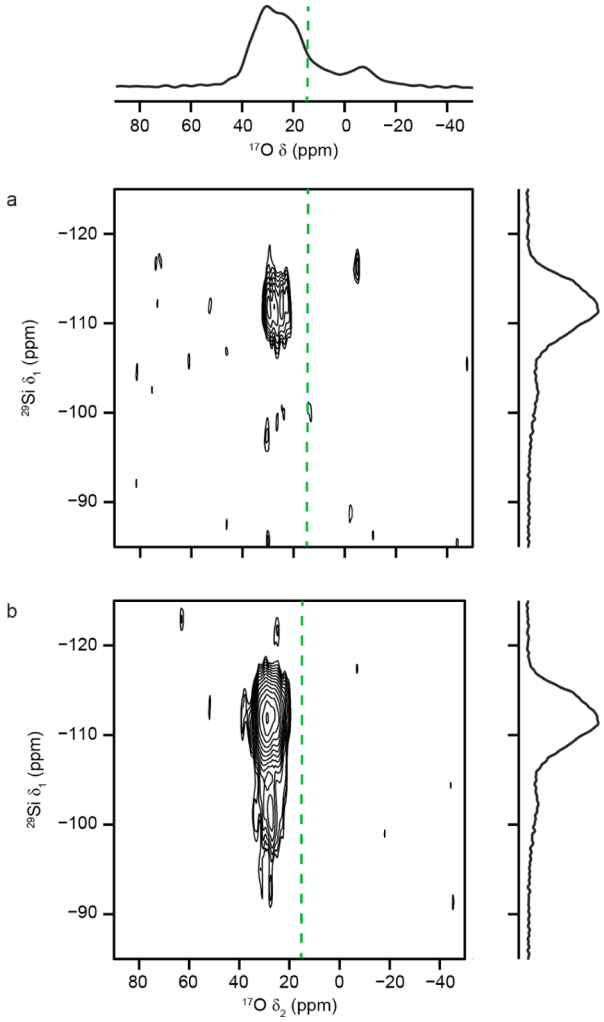

Figure 10. $^{17}O-^{29}Si$ (20.0 T, 20 kHz MAS) D-HMQC correlation spectra of ^{29}Si-enriched Ge-UTL hydrolyzed with ^{17}O-enriched H_2O for 16 h, acquired using (a) τ = 600 μs and (b) τ = 2400 μs of $SR4^2_1$ recoupling. Also shown (for comparison) are the ^{17}O and ^{29}Si MAS NMR spectra. The dashed green line denotes the position of maximum signal intensity for the Si−OH species identified using CP experiments.

CONCLUSIONS

The successful synthesis of isotopically enriched IPC-2P ADOR intermediate and IPC-2 zeolite has been demonstrated, and mechanistic studies provide new insight into the hydrolytic rearrangement that underpins the ADOR philosophy. The use of a lower volume of hydrolysis for the reaction to enable economic isotopic enrichment varies the reaction rate and the products obtained at each step, demonstrating the sensitivity of the ADOR process to a variety of experimental conditions and, therefore, the fine control of the reaction progression that may be possible. The work allows us to draw a modified mechanism (Figure 11) suitable for these low hydrolysis volume situations that differs from that shown in Figure 1 in that the hydrolysis to IPC-1P never goes to completion before the organization step begins. Both ^{29}Si and ^{17}O NMR spectroscopies have demonstrated that the hydrolysis and rearrangement process occurs over a much longer time scale than seen by diffraction (where a constant d spacing is observed at very short durations). ^{29}Si MAS NMR spectra showed (through a consideration of the Q^4/Q^3 intensities) that for the first ∼12 h of reaction, hydrolysis was the dominant process, with subsequent rearrangement still occurring up to ∼48 h. However, ^{17}O MAS NMR spectra of zeolites enriched in ^{17}O during the hydrolysis step showed changes of the spectral line shape over a much longer time scale (∼30 days), reflecting a low level of ongoing hydrolysis even at room temperature, most likely as a result of the small amount of acid remaining between the layers, owing to the reduced volume of (unenriched) washing water used.

^2H MAS NMR suggested that there are around 2−4 D_2O molecules for every Si−OD species in the interlayer region, although this amount does vary with reaction duration and storage conditions. Two main signals were observed in ^{17}O MAS NMR spectra of the enriched zeolites, attributed to Si−O−Si and Si−OH species (along with signal for H_2O itself). MQMAS, CP, and spin-locking experiments were able to provide information on the spectral line shapes of the different components, enabling their relative proportions (8:1 for Si−^{17}O−Si:Si−^{17}OH) to be determined from the MAS spectrum.

The unexpectedly high proportion of Si−O−Si species enriched in ^{17}O (even allowing for faster back exchange of Si−OH groups) highlighted a much more extensive hydrolytic rearrangement than previously thought. Heteronuclear ($^{17}O-^{29}Si$) correlation experiments confirmed that a substantial amount of ^{17}O was incorporated into a bulk of the layers of the IPC-2P zeolite, rather than being confined only to the hydrolyzed interlayer regions. The ability to exploit isotopic enrichment (in both ^{29}Si and ^{17}O) of these materials has not only enabled a more detailed spectroscopic investigation but also has provided new insight into the ADOR mechanism and the possible ways in which zeolite structures could be more accurately targeted in the future.

DOI: 10.1021/jacs.7b00386
J. Am. Chem. Soc. 2017, 139, 5140−5148

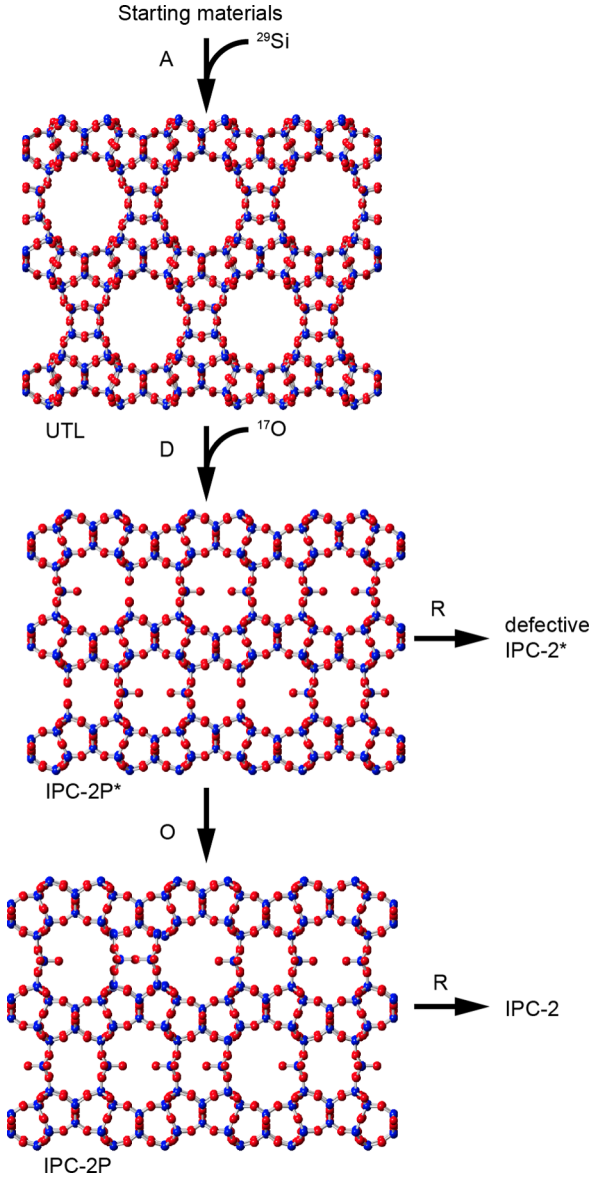

Figure 11. Modified ADOR process suitable for situations where there is a lower volume of hydrolysis solution and where full hydrolysis of the solution to IPC-1P never goes to completion before the organization step begins. Instead, the defective IPC-2P* is formed, which slowly transforms to a more ideal form of IPC-2P. The steps in which isotropic enrichment is introduced are also shown. Color key: Si = blue, O = red.

■ ASSOCIATED CONTENT

Supporting Information

The Supporting Information is available free of charge on the ACS Publications website at DOI: 10.1021/jacs.7b00386.

Further synthetic details, information on XRD measurements, variable-field ^{17}O MAS and MQMAS spectra, information on $T_{1\rho}$ measurements and spin-locking behavior, ^{2}H MAS experiments, the decomposition of the ^{17}O MAS spectrum, and the synthesis and characterization of amorphous $Si^{17}O_2$ (PDF)

■ AUTHOR INFORMATION

Corresponding Authors

*sema@st-andrews.ac.uk

*rem1@st-andrews.ac.uk

ORCID

Sharon E. Ashbrook: 0000-0002-4538-6782

Notes

The authors declare no competing financial interest.

■ ACKNOWLEDGMENTS

We would like to thank the ERC (EU FP7 Consolidator Grant 614290 "EXONMR"), the Leverhulme Trust (IN-2012-094), and EPSRC (EP/K025112/1, EP/L014475/1, and EP/M506631/1 (for GPMB)). S.E.A. would like to thank the Royal Society and the Wolfson Foundation for a merit award. The UK 850 MHz solid-state NMR Facility used in this research was funded by EPSRC and BBSRC (contract reference PR140003) as well as the University of Warwick including via part funding through Birmingham Science City Advanced Materials Projects 1 and 2 supported by Advantage West Midlands (AWM) and the European Regional Development Fund (ERDF). Collaborative assistance from the 850 MHz Facility Manager (Dinu Iuga, University of Warwick) is acknowledged. The University of Nottingham DNP MAS NMR Facility used in this research was funded by EPSRC and the University of Nottingham, and assistance from the Facility Manager (Subhradip Paul, University of Nottingham) is also acknowledged. The research data (and/or materials) supporting this publication can be accessed at DOI: 10.17630/d66d1146-5892-4f14-8e41-dfc075a8cd91.

■ REFERENCES

(1) Wright, P. A. *Microporous Framework Solids*; RSC Publishing: Cambridge, 2008.
(2) Davis, M. E. *Nature* **2002**, *417*, 813−821.
(3) Primo, A.; Garcia, H. *Chem. Soc. Rev.* **2014**, *43*, 7548−7561.
(4) Martínez, C.; Corma, A. *Coord. Chem. Rev.* **2011**, *255*, 1558−1580.
(5) Gascon, J.; Kapteijn, F.; Zornoza, B.; Sebastián, V.; Casado, C.; Coronas, J. *Chem. Mater.* **2012**, *24*, 2829−2844.
(6) Cheung, O.; Hedin, N. *RSC Adv.* **2014**, *4*, 14480−15.
(7) Moliner, M. *Dalton Trans.* **2014**, *43*, 4197−4208.
(8) Li, K.; Valla, J.; Garcia-Martinez, J. *ChemCatChem* **2014**, *6*, 46−66.
(9) Pina, M. P.; Mallada, R.; Arruebo, M.; Urbiztondo, M.; Navascués, N.; de la Iglesia, O.; Santamaria, J. *Microporous Mesoporous Mater.* **2011**, *144*, 19−27.
(10) Babaei, A.; Khalilzadeh, B.; Afrasiabi, M. *J. Appl. Electrochem.* **2010**, *40*, 1537−1543.
(11) Jiang, J.; Jorda, J. L.; Yu, J.; Baumes, L. A.; Mugnaioli, E.; Diaz-Cabanas, M. J.; Kolb, U.; Corma, A. *Science* **2011**, *333*, 1131−1134.
(12) Baerlocher, C.; Weber, T.; McCusker, L. B.; Palatinus, L.; Zones, S. I. *Science* **2011**, *333*, 1134−1137.
(13) Simancas, R.; Dari, D.; Velamazán, N.; Navarro, M. T.; Cantín, A.; Jordá, J. L.; Sastre, G.; Corma, A.; Rey, F. *Science* **2010**, *330*, 1219−1222.
(14) Sun, J.; Bonneau, C.; Cantín, A.; Corma, A.; Diaz-Cabanas, M. J.; Moliner, M.; Zhang, D.; Li, M.; Zou, X. *Nature* **2009**, *458*, 1154−1157.
(15) Choi, M.; Na, K.; Kim, J.; Sakamoto, Y.; Terasaki, O.; Ryoo, R. *Nature* **2009**, *461*, 246−249.
(16) Na, K.; Choi, M.; Park, W.; Sakamoto, Y.; Terasaki, O.; Ryoo, R. *J. Am. Chem. Soc.* **2010**, *132*, 4169−4177.
(17) Varoon, K.; Zhang, X.; Elyassi, B.; Brewer, D. D.; Gettel, M.; Kumar, S.; Lee, J. A.; Maheshwari, S.; Mittal, A.; Sung, C.-Y.; Cococcioni, M.; Francis, L. F.; McCormick, A. V.; Mkhoyan, K. A.; Tsapatsis, M. *Science* **2011**, *334*, 72−75.

DOI: 10.1021/jacs.7b00386
J. Am. Chem. Soc. 2017, 139, 5140−5148

(18) Zhang, X.; Liu, D.; Xu, D.; Asahina, S.; Cychosz, K. A.; Agrawal, K. V.; Al Wahedi, Y.; Bhan, A.; Al Hashimi, S.; Terasaki, O.; Thommes, M.; Tsapatsis, M. *Science* **2012**, *336*, 1684−1687.
(19) Pophale, R.; Cheeseman, P. A.; Deem, M. W. *Phys. Chem. Chem. Phys.* **2011**, *13*, 12407−12412.
(20) Foster, M. D.; Simperler, A.; Bell, R. G.; Friedrichs, O. D.; Paz, F. A. A.; Klinowski, J. *Nat. Mater.* **2004**, *3*, 234−238.
(21) Roth, W. J.; Nachtigall, P.; Morris, R. E.; Wheatley, P. S.; Seymour, V. R.; Ashbrook, S. E.; Chlubná, P.; Grajciar, L.; Položij, M.; Zukal, A.; Shvets, O.; Čejka, J. *Nat. Chem.* **2013**, *5*, 628−633.
(22) Morris, R. E.; Čejka, J. *Nat. Chem.* **2015**, *7*, 381−388.
(23) Eliášová, P.; Opanasenko, M.; Wheatley, P. S.; Shamzhy, M.; Mazur, M.; Nachtigall, P.; Roth, W. J.; Morris, R. E.; Čejka, J. *Chem. Soc. Rev.* **2015**, *44*, 7177−7206.
(24) Wheatley, P. S.; Chlubná-Eliášová, P.; Greer, H.; Zhou, W.; Seymour, V. R.; Dawson, D. M.; Ashbrook, S. E.; Pinar, A. B.; McCusker, L. B.; Opanasenko, M.; Čejka, J.; Morris, R. E. *Angew. Chem., Int. Ed.* **2014**, *53*, 13210−13214.
(25) Roth, W. J.; Nachtigall, P.; Morris, R. E.; Čejka, J. *Chem. Rev.* **2014**, *114*, 4807−4837.
(26) Blasco, T.; Corma, A.; Díaz-Cabañas, M. J.; Rey, F.; Vidal-Moya, J. A.; Zicovich-Wilson, C. M. *J. Phys. Chem. B* **2002**, *106*, 2634−2642.
(27) Jiang, J.; Jordá, J. L.; Diaz-Cabanas, M. J.; Yu, J.; Corma, A. *Angew. Chem., Int. Ed.* **2010**, *49*, 4986−4988.
(28) Corma, A.; Navarro, M. T.; Rey, F.; Rius, J.; Valencia, S. *Angew. Chem.* **2001**, *113*, 2337−2340.
(29) Verheyen, E.; Joos, L.; Van Havenbergh, K.; Breynaert, E.; Kasian, N.; Gobechiya, E.; Houthoofd, K.; Martineau, C.; Hinterstein, M.; Taulelle, F.; Van Speybroeck, V.; Waroquier, M.; Bals, S.; Van Tendeloo, G.; Kirschhock, C. E. A.; Martens, J. A. *Nat. Mater.* **2012**, *11*, 1059−1064.
(30) Roth, W. J.; Shvets, O. V.; Shamzhy, M.; Chlubná, P.; Kubu, M.; Nachtigall, P.; Čejka, J. *J. Am. Chem. Soc.* **2011**, *133*, 6130−6133.
(31) Ravenelle, R. M.; Schüβler, F.; D'Amico, A.; Danilina, N.; van Bokhoven, J. A.; Lercher, J. A.; Jones, C. W.; Sievers, C. *J. Phys. Chem. C* **2010**, *114*, 19582−19595.
(32) Corma, A.; Díaz-Cabañas, M. J.; Rey, F.; Nicolopoulus, S.; Boulahya, K. *Chem. Commun.* **2004**, 1356−1357.
(33) Paillaud, J. L.; Harbuzaru, B.; Patarin, J.; Bats, N. *Science* **2004**, *304*, 990−992.
(34) Mazur, M.; Wheatley, P. S.; Navarro, M.; Roth, W. J.; Položij, M.; Mayoral, A.; Eliášová, P.; Nachtigall, P.; Čejka, J.; Morris, R. E. *Nat. Chem.* **2015**, *8*, 58−62.
(35) Cundy, C. S.; Cox, P. A. *Chem. Rev.* **2003**, *103*, 663−702.
(36) Cundy, C. S.; Cox, P. A. *Microporous Mesoporous Mater.* **2005**, *82*, 1−78.
(37) Morris, S. A.; Wheatley, P. A.; Položij, M.; Nachtigall, P.; Eliášová, P.; Čejka, J.; Lucas, T. M.; Hriljac, J. A.; Pinar, A. B.; Morris, R. E. *Dalton Trans.* **2016**, *45*, 14124−14130.
(38) Ashbrook, S. E.; Dawson, D. M.; Seymour, V. R. *Phys. Chem. Chem. Phys.* **2014**, *16*, 8223−8242.
(39) Mafra, L.; Klinowski, J. *Molecular Sieves: Crystalline Systems, eMagRes.* **1996**, DOI: 10.1002/9780470034590.emrstm1325.
(40) Mafra, L.; Klinowski, J. *Advanced Solid State NMR Techniques for the Study of Molecular Sieves, eMagRes.* **1996**, DOI: 10.1002/9780470034590.emrstm1307.
(41) Hunger, M. *Catal. Rev.: Sci. Eng.* **1997**, *39*, 345−393.
(42) Zhang, W.; Xu, S.; Han, X.; Bao, X. *Chem. Soc. Rev.* **2012**, *41*, 192−210.
(43) Ashbrook, S. E.; Dawson, D. M.; Griffin, J. M. *Solid-State NMR in Local Structural Characterisation*; Bruce, D. W., O'Hare, D., Walton, R. I., Eds.; John Wiley & Sons Ltd: Chichester, U.K., 2014.
(44) Ashbrook, S. E.; Sneddon, S. *J. Am. Chem. Soc.* **2014**, *136*, 15440−15456.
(45) Massiot, D.; Fayon, F.; Capron, M.; King, I.; Le Calve, S.; Alonso, B.; Durand, J. O.; Bujoli, B.; Gan, Z.; Hoatson, G. *Magn. Reson. Chem.* **2002**, *40*, 70−76.
(46) Pines, A.; Gibby, M. G.; Waugh, J. S. *J. Chem. Phys.* **1972**, *56*, 1776−1777.
(47) Frydman, L.; Harwood, J. S. *J. Am. Chem. Soc.* **1995**, *117*, 5367−5368.
(48) Amoureux, J. P.; Fernandez, C.; Steuernagel, S. *J. Magn. Reson., Ser. A* **1996**, *123*, 116−118.
(49) Brown, S. P.; Wimperis, S. *J. Magn. Reson.* **1997**, *128*, 42−61.
(50) Pike, K. J.; Malde, R. P.; Ashbrook, S. E.; McManus, J.; Wimperis, S. *Solid State Nucl. Magn. Reson.* **2000**, *16*, 203−215.
(51) Brinkmann, A.; Kentgens, A. P. M. *J. Am. Chem. Soc.* **2006**, *128*, 14758−14759.
(52) Amoureux, J. P.; Trebosc, J.; Delevoye, L.; Lafon, O.; Hu, B.; Wang, Q. *Solid State Nucl. Magn. Reson.* **2009**, *35*, 12−18.
(53) Morris, S. A.; Bignami, G. P. M.; Tian, Y.; Navarro, N.; Firth, D. S.; Cejka, J.; Wheatley, P. S.; Dawson, D. M.; Wojciech, A. S.; Wragg, D. S.; Morris, R. E.; Ashbrook, S. E. *Nature Chem.*, in press.
(54) Ashbrook, S. E.; Wimperis, S. *Mol. Phys.* **2000**, *98*, 1−26.
(55) Ashbrook, S. E.; Wimperis, S. *J. Chem. Phys.* **2004**, *120*, 2719−2731.
(56) Ashbrook, S. E.; Wimperis, S. *J. Chem. Phys.* **2009**, *131*, 194509.

DOI: 10.1021/jacs.7b00386
J. Am. Chem. Soc. 2017, 139, 5140−5148